GAS-PRODUCING CHARACTERISTICS OF COALS CONTAINING HYDROGEN SULFIDE BY THE THERMOCHEMICAL SULFATE REDUCTION

by

Qigen DENG[a,b,c*], Jingping YIN[a,b], Tao ZHANG[a,b], and Hao WANG[a,b]

[a] State Key Laboratory Cultivation Base for Gas Geology and Gas Control, Henan Polytechnic University, Jiaozuo, Henan, China
[b] School of Safety Science and Engineering, Henan Polytechnic University, Jiaozuo, Henan, China
[c] Collaborative Innovation Centre of Coal Safety Production of Henan Province, Jiaozuo, Henan, China

Original scientific paper
https://doi.org/10.2298/TSCI2004475D

It is generally considered that the thermochemical sulfate reduction is one of the main origins of high content of hydrogen sulfide (H_2S). Thermochemical sulfate reduction simulation experiments at different temperatures ranging from 200 ℃ to 600 ℃ were carried out to study the output of gaseous products, which include CO_2, CH_4, H_2S, and heavy hydrocarbon (C_{2-6}). Thermochemical sulfate reduction can promote the formation of CH_4 and H_2S, and can preferentially consume heavy hydrocarbons. The CH_4 is difficult to participate in the reaction of formation H_2S. The concentrations of CO_2 and hydrogen are closely related to the evolution characteristics of H_2S. The intermediate sulfur-containing products from thermochemical reaction and thermal cracking of coals can promote the progress of thermochemical sulfate reduction and possible formation of H_2S.

Key words: *coal, thermochemical sulfate reduction, simulation experiment, H_2S, gas products, evolution characteristic*

Introduction

In a coal mining, abnormal emissions and accidents aroused by the high content of H_2S occur frequently [1-3]. It is widely believed that the thermochemical sulfate reduction (TSR) is one of the main factors of high H_2S content in coal seams, and the TSR has been proposed and accepted as the principal source of H_2S and predominant mechanism for high-quality deeply-buried hydrocarbon reservoirs rich in H_2S around the world, especially for deep carbonate gas reservoirs [4-6]. While TSR simulation experiment can be conducted under well-defined conditions to exclude many interference factors in geological conditions, directly aiming at reaction mechanism and control conditions. Although it is difficult for laboratory TSR experiment to simulate conditions resembling nature, it is still one of the most important methods to enhance the understanding of detailed TSR process. At present, different kinds of TSR simulation experiments were carried out to study the influence of threshold temperature, sulfate species, pH, hydrocarbon type, and H_2S presence on TSR reaction [1, 7-9]. Besides, simulation experiments provide systematic isotopic and yield data to study the kinetic process of TSR, which can extend the experimental results to different geologic condi-

* Corresponding author, e-mail: dengqigen@hpu.edu.cn

tions. This paper will use a reaction device under high pressure and high temperature to carry out thermal simulation experiment under different medium conditions to explore the gas-producing characteristics of coals containing H_2S, so that the formation and enrichment of H_2S in a coal rock can be elucidated. The original formation of H_2S in coal and rock is beneficial to the prevention and control of H_2S in coal mines.

Experimental samples

The coal samples used in the experiment were collected from Xishan Coal Mine and Liuhuanggou Coal Mine, the Jurassic Xishanyao Formation in Urumqi, China, where H_2S is abnormally enriched. The parameters were tested, and the results were shown in tab. 1, where, M_{ad} is air-dried moisture, A_d is ash dry, V_{daf} is dry-ash-free volatile, $S_{t,d}$ is dry basis total sulfur, $S_{o,d}$ is dry basis organic sulfur, $S_{p,d}$ is dry basis pyretic sulfur, R_0 is vitrinite reflectance of coal, XS1 and XS2 are coal samples of Xishan Coal Mine, and LHG1 is coal sample 1 of Liuhuanggou Coal Mine.

Table 1. Test results of experimental samples

Samples	Proximate analysis [%]			Ultimate analysis [%]			Sulfur composition [%]				R_0 [%]
	M_{ad}	A_d	V_{daf}	C	H	N	O	$S_{t,d}$	$S_{o,d}$	$S_{p,d}$	
XS1	4.20	8.14	39.56	82.97	6.36	1.32	7.81	3.16	0.75	2.41	0.69
XS2	3.01	9.35	39.84	82.01	5.85	1.40	9.92	1.74	0.78	0.96	0.56
LHG1	3.49	13.89	40.93	83.69	5.03	1.33	8.69	1.21	0.43	0.78	0.47

Experimental instruments and methods

The experiment system mainly includes a vacuum degasser, a loading device, a pyrolysis device, a gas collector and an analyzing apparatus [7]. The highest temperature of the reactor can reach 650 ℃, and the temperature control accuracy is ±1 ℃. The highest pressure of this reactor can reach 25.0 MPa, and the control accuracy is ±0.5 MPa. The diagram of experimental instrument is illustrated in fig. 1.

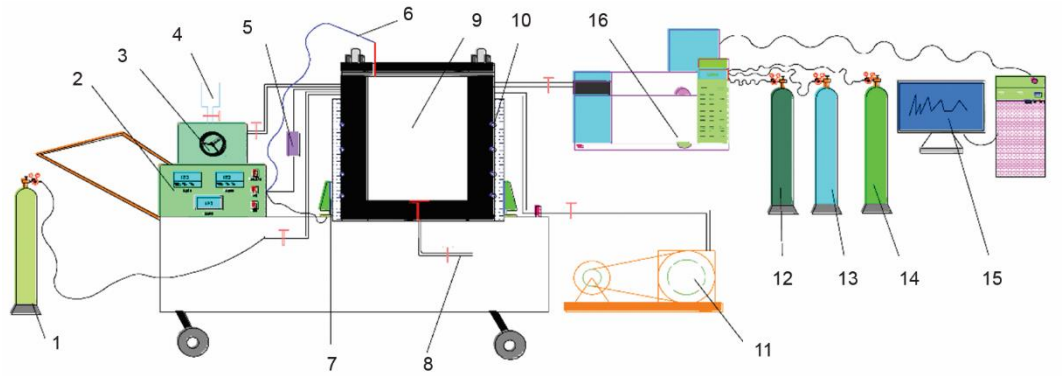

Figure 1. Diagram of experimental instruments; *1, 12, 13, 14 – carrier gas cylinder, 2 – controller, 3 – pressure device, 4 – loading device for liquid, 5 – pressure sensor, 6 – temperature measuring device, 7 – water circulating cooling device, 8 – liquid outlet, 9 – the body of reactor, 10 – cooling circulating hole, 11 – vacuum pump, 15 – computer, 16 – gas chromatograph or micro-coulomb titration*

A coal sample of 1000 g was put into the reactor, and the helium was used to wash repeatedly each sample to remove the air sealed in the reactor for 12 hours until the vacuum degree was less than 20 Pa. Then the underground water of 500 mL was injected into the reactor. The initial pressure in the reactor was set to 5.0 MPa, the final pressure ranged from 12.0 MPa to 20.0 MPa. The heating rate was 20 ℃ per hour, the temperature ranged from 200 ℃ to 600 ℃. Gases were collected at nine temperature spots: 200 ℃, 250 ℃, 300 ℃, 350 ℃, 400 ℃, 450 ℃, 500 ℃, 550 ℃, and 600 ℃, respectively. The heating time was set to 24 hours in each stage of each experiment.

Experimental result

Output of CH_4

The concentration change of CH_4 *vs.* temperature was shown in fig. 2. When the temperature was less than 250 ℃, CH_4 was mainly released from desorbed coals. At the stage of 300-500 ℃, the formation of CH_4 was mainly related to the shedding of fat side chains and the removal of oxygen-containing functional groups. After 500 ℃, CH_4 was mainly formed by cracking of short-chain fat structure and aromatization and polycondensation of cyclic alkanes. The yield of CH_4 was not high at the beginning of the reaction. Subsequently, the output of CH_4 increased sharply, indicating that the temperature controls the amount of CH_4, and the TSR effect promotes the formation of methane [8-10]. Its reaction equations can be shown:

$$(C_6H_5)OCH_3 \rightarrow (C_6H_5)O\bullet + CH_3\bullet \tag{1}$$

$$CH_3\bullet + (C_6H_5)OCH_3 \rightarrow CH_4 + (C_6H_5)OCH_2\bullet \tag{2}$$

Output of heavy hydrocarbon

The output of heavy hydrocarbon ($C_{2\text{-}6}$) mainly including C_2H_6 and C_3H_8 at different temperatures was shown in fig. 3. When the temperature was changed from 350 ℃ to 450 ℃, the output of $C_{2\text{-}6}$ was highest. The $C_{2\text{-}6}$ was mainly produced from the -OHOH reaction formed by the -OH reaction at the intermediate position of the carbon atom in the aliphatic hydrocarbon chain [11, 12]. Its reaction equations can be shown:

$$R - C(OH)_2 - CH_2 - CH_3 \rightarrow R - COOH + C_2H_6 \tag{3}$$

$$R - CH_2 - C(OH)_2 - CH = CH_2 \rightarrow R - CH_2 - COOH + C_2H_4 \tag{4}$$

$$R - CH_2 - C(OH)_2 - CH_2 - CH_2 - CH_3 \rightarrow R - CH_2 - COOH + C_3H_8 \tag{5}$$

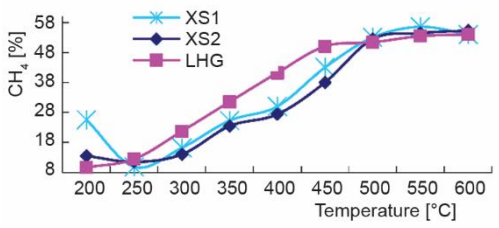

Figure 2. Variation characteristics of gas components of CH_4

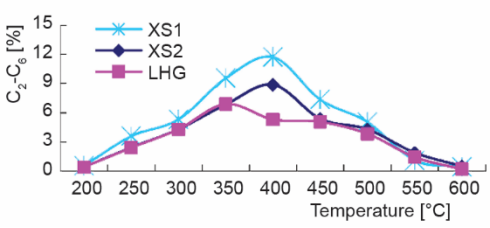

Figure 3. Variation characteristics of heavy hydrocarbon ($C_{2\text{-}6}$)

When the temperature was larger than 400 ℃, TSR accelerated the reaction of heavy hydrocarbons, $C_{2\text{-}6}$, with compounds contained with sulfur, $C_{2\text{-}6}$ began to undergo secondary cracking, resulting in a significant decrease in the output of $C_{2\text{-}6}$. Its possible reaction equations can be shown:

$$3S^0 + C_2H_6 + 2H_2O \rightarrow 3H_2S + CH_4 + CO_2 \tag{6}$$

$$6S^0 + C_3H_8 + 4H_2O \rightarrow 6H_2S + CH_4 + 2CO_2 \tag{7}$$

$$6C_nH_{2n+2} + (4n+2)SO_4^{2-} \rightarrow (4n+2)O^{2-} + (5n+1)CO_2 + \\ +(4n+2)H_2S + (2n+4)H_2 + (n-1)C, \quad n = (1,2,3\ldots) \tag{8}$$

Output of H_2S

The output of H_2S was changed with temperature as shown in fig. 4. When the temperature was less than 300 ℃, the output was low and changed slowly, indicating that TSR was very weak, a small amount of H_2S might come from the unstable organic sulfur (such as thioether, mercaptan, and disulfide) [13-16]. With the development of thermal evolution, the output decreased rapidly. When the temperature reached higher than 450 ℃ or 500 ℃, the output decreased with the increase of the temperature.

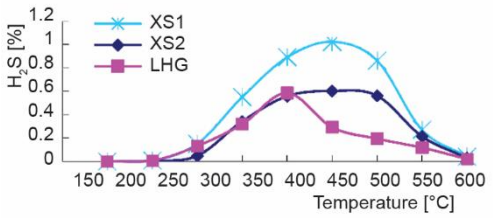

Figure 4. Variation characteristics of H_2S

In the reaction stage of 350-500 ℃, the hydrogen radicals induced the cracking of aromatic rings, including the breakage of side chains, aliphatic chains, ether bonds and mercaptans. A large amount of sulfur radical fragments was produced, and H_2S was formed when combined with hydrogen radicals. Its possible reaction equations can be shown:

$$2RSH \rightarrow R_2S + H_2S \tag{9}$$

$$RSSR' + RH \rightarrow RSR' + H_2S \tag{10}$$

The maximal output at the stage of 450-500 ℃ indicated that the pyrite begins to be decomposed. The decomposition of pyrite can generate intermediate products such as FeS, COS, H_2S, and S^0, which can be further reacted to generate H_2S. As shown:

$$FeS_2 + CO \rightarrow FeS + COS \tag{11}$$

$$FeS_2 \rightarrow FeS + S \tag{12}$$

$$S + CO \rightarrow COS \tag{13}$$

$$COS + H_2 \rightarrow CO + H_2S \tag{14}$$

$$COS + H_2O \rightarrow CO_2 + H_2S \tag{15}$$

In the 450/500-600 ℃ stage, H_2S was mainly formed from sulfur reduction of thiophene structure. The conversion reaction was as shown:

$$RCH_2CH_3 + S^0 \rightarrow RCH = RCH_2 + H_2S \quad (16)$$

$$RCH_3 + 3S^0 + 2H_2O \rightarrow RCHOOH + 3H_2S \quad (17)$$

$$2RH + 2S^0 \rightarrow RSR + H_2S \quad (18)$$

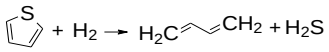

(19)

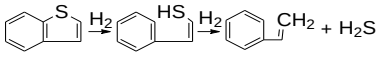

(20)

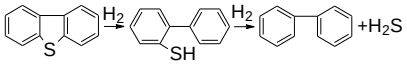

(21)

After 600 ℃, the output of H_2S was very low. It may be due to the gradual consumption of available sulfur radicals in the coal. The H_2S may be derived from decomposition reactions of organic aliphatic thiols, disulfides, *etc.* in coal. The conversion reaction was as shown:

$$RSH + H_2O \rightarrow ROH + H_2S \quad (22)$$

In the stage of large amount of hydrogen sulfide generation, CH_4 was not only consumed, but also increased, while heavy hydrocarbon gas saw a downward trend, indicating that CH_4 was rarely involved in the hydrogen sulfide reaction, and TSR reaction preferentially consumed heavy hydrocarbons.

Output of CO_2

The output of CO_2 was shown in fig. 5. The oxygen-containing functional groups in coals mainly include carboxyl group, phenol carboxyl group, mercapto group, methoxy group, ether bond and hetero-epoxy group. It is generally considered that CO_2 was produced from the thermal decomposition of oxygen-containing functional group such as carboxyl group or ester in coals [17, 18]. The carboxyl group decomposes to form CO_2 at a temperature above 200 ℃, and a large amount of CO_2 was derived from the desorption of the adsorbed state in the raw coal, so that the maximum amount of CO_2 can be released at a lower temperature. In the high temperature stage, CO_2 was mainly formed by decarboxylation of fatty acids by heat. After the deep TSR happened at the temperature of 450 ℃, the output of CO_2 changed from decreasing steadily to rising slowly, therefore, to some extent, CO_2 can represent the reaction progress of TSR, reflecting the positive correlation. In addition, the sulfur element formed during the reaction easily reacts with hydrocarbons to form H_2S and CO_2. The conversion reaction was as shown in eqs. (23)-(25):

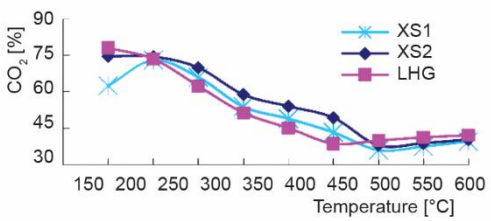

Figure 5. Variation characteristics of CO_2

$$4S^0 + 1.33(-CH_2) + 2.67H_2O \rightarrow 4H_2S(g) + 1.33CO_2 \quad (23)$$

$$RCOOH \rightarrow RH + CO_2 \tag{24}$$

$$Ar - COOH + HOOC - Ar \rightarrow Ar - O - Ar + H_2O + CO_2 \tag{25}$$

where Ar represents an aromatic ring in the coal macromolecule.

Output of H_2

The output of H_2 was given in fig. 6. The hydrogen release was mainly the result of polycondensation and dehydrogenation of aromatic structures in coals [19]. Before 450 ℃, H_2 was formed mainly by dehydrogenation of the aliphatic side chain connected with the oxygen-containing functional group in the coal macromolecular structure. After 500 ℃, as the pyrolysis temperature increases, the aromatic ring with a smaller number of rings transformed into a more fused aromatic hydrocarbon with a larger number of rings, and the cyclodeductive dehydrogenation of polycyclic concentration occurred, resulting in the formation of hydrogen [20, 21]. When the temperature was between 300 ℃ and 450 ℃, the H_2 content decreased remarkably, the possible reason was that the TSR had occurred between the sulfur free radicals in coals and the generated H_2, resulting in the generation of H_2S, thereby leading to the decrease of the output of H_2. When the temperature was higher than 300 ℃ and lower than 450 ℃, since H_2 produced by the breakage of C-H bond might react with sulfur free radicals firstly, and was transferred immediately, resulting in the generation of H_2S, thereby leading to the decrease of the output of H_2. After the temperature of 450 ℃, it was probably because the sulfur free radicals in coals were consumed and could not be provided sufficiently, resulting in the rise of the output of H_2. The conversion reaction was as shown:

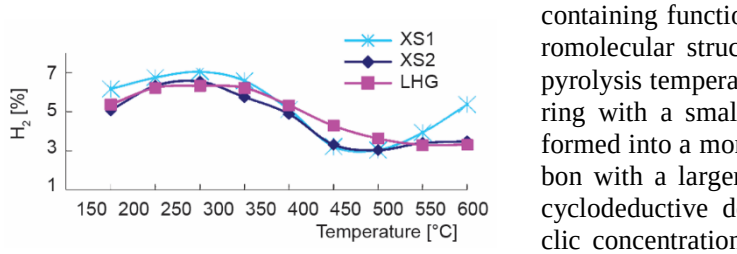

Figure 6. Variation characteristics of H_2

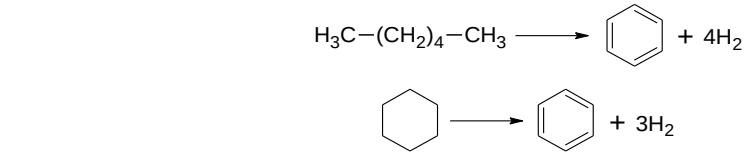

(26)

(27)

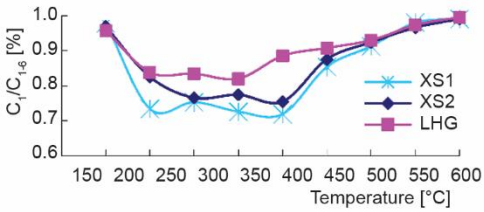

Figure 7. Characteristics of aridity coefficient

Change characteristic of aridity coefficient (C_1/C_{1-6})

The characteristics of aridity coefficient was shown in fig. 7. With the progress of thermal evolution, before the temperature of 350-400 ℃, the aridity coefficient presented a decreased trend, and increased gradually thereafter. But the productive rate of CH_4 in the process of thermal evolution increased steadily. So the decrease of aridity coefficient before 350-450 ℃ was probably caused by the rapid growth of gases of C_{1-6} components, and the aridity coefficient increased after 350-450 ℃, the reason may be that gases of C_{1-6} were involved in the TSR to generate H_2S, and the heavy hydrocarbon was consumed constantly [12, 22-24].

Conclusions

It is generally believed that TSR is one of the main causes of high content of H_2S in coal seams, TSR can distinctly prompt the thermal cracking and thermal chemical reduction reaction of coals.

The TSR has a significant modification effect on the composition of gaseous products, it can promote the formation of CH_4 and H_2S, and can preferentially consume heavy hydrocarbons. It was difficult for CH_4 to participate the TSR to formation of H_2S. The characteristics of CO_2 and hydrogen change were closely related to the evolution characteristics of H_2S. The thermochemical reaction or thermal cracking intermediate of the coal, mercaptan, and sulfide can promote the progress of the TSR and form H_2S. The higher the sulfur content in the coal, the more H_2S was formed. The occurrence of TSR was accompanied with the generation of heavy hydrocarbon, the most drastic stage of TSR was also the stage that generates the largest amount of heavy hydrocarbon gases.

In recent years, there were a lot of consensus on the new understanding of the thermochemical reduction mechanism of coal sulfate and the newly formed organic compounds. In the future, attention should be paid to the impact of TSR on the evolution or formation of coal, and the use of computer simulation to reproduce TSR process research, and the fractal calculus [25-35] can be effectively applied to study the effect of the porous structure on the gas release property.

Acknowledgment

This work was supported by National Natural Science Foundation of China under the grant Nos. 51774116 and U1504403 and Postdoctoral Research Fund of Henan Province under the grant No. 001703031. The authors are also grateful to Professor Mingju LIU of Henan Polytechnic University for his ardent guidance and help.

References

[1] Cai, C. F., *et al.*, Relative Reactivity of Saturated Hydrocarbons During Thermochemical Sulfate Reduction, *Fuel, 253* (2019), Oct., pp. 106-113
[2] Geoffrey S., *et al.*, Effects of Thermal Maturation and Thermochemical Sulfate Reduction on Compound-Specific Sulfur Isotopic Compositions of Organosulfur Compounds in Phosphoria Oils from the Bighorn Basin, USA, *Organic Geochemistry, 103* (2017), 1, pp. 63-78
[3] Deng Q. G., *et al.*, A Study of Hydrogen Sulfide Genesis in Coal Mine of Southeastern Margin of Junggar Basin, (in Chinese), *Earth Science Frontiers, 24* (2017), 5, pp. 395-401
[4] Liu, M. J., et al., Origin of Hydrogen Sulfide in Coal Seams in China, *Safety Science, 50* (2012), 4, pp. 1031-1038
[5] Deng, Q. G., *et al.*, Research Advances of Prevention and Control of Hydrogen Sulfide in Coal Mines, *The Scientific World Journal, 2019* (2019), ID 8719260
[6] Biehl, B. C., *et al.*, Impacts of Hydrothermal Dolomitization and Thermochemical Sulfate Reduction on Secondary Porosity Creation in Deeply Buried Carbonates: A Case Study from the Lower Saxony Basin, Northwest Germany, *Am. Assoc. Pet. Geol. Bull, 100* (2016), 4, pp. 597-621
[7] Deng, Q. G., *et al.*, Thermal Simulation Experiment and Research on the System of coal/coal & water/coal & water & $MgSO_4$/coal & water & $CaSO_4$, *Desalination and Water Treatment, 149* (2019), 5, pp. 388-397
[8] Cross, M. M., *et al.*, Thermochemical Sulphate Reduction (TSR): Experimental Determination of Reaction Kinetics and Implications of the Observed Reaction Rates for Petroleum Reservoirs, *Organic Geochemistry, 35* (2004), 4, pp. 393-404
[9] Zhang, P. W., *et al.*, Alteration of Solid Bitumen by Hydrothermal Heating and Thermochemical Sulfate Reduction in the Ediacaran and Cambrian Dolomite Reservoirs in the Central Sichuan Basin, SW China, *Precambrian Research, 321* (2018), 2, pp. 277-302

[10] Wu, B. X., *et al.*, Study on Gas Generation from Low Maturity Asphalt in Sichuan Basin, *Journal of China Coal Society, 38* (2013), 5, pp. 748-753
[11] Michael G., *et al.*, The World-Class Howard's Pass SEDEX Zn-Pb District, Selwyn Basin, Yukon, Part II: The Roles of Thermochemical and Bacterial Sulfate Reduction in Metal Fixation, *Mineralium Deposita*, *52* (2017), 3, pp. 405-419
[12] Xiao, Q. L., *et al.*, The Effects of Selected Minerals on Laboratory Simulated Thermochemical Sulfate Reduction. *Organic Geochemistry, 122* (2018), 8, pp. 41-45
[13] Geoffrey S., *et al.*, Effects of Thermal Maturation and Thermochemical Sulfate Reduction on Compound-Specific Sulfur Isotopic Compositions of Organosulfur Compounds in Phosphoria Oils from the Bighorn Basin, USA, *Organic Geochemistry, 103* (2017), 1, pp. 63-78
[14] Lin, R. Y., *et al.*, Hydrogen Suifide Formation Mechanism in the Process of Thermal Recovery, *Acta Petrolei Sinica in Chinese, 35* (2014), 6, pp. 1153-1159
[15] Zhang, J. Y., *et al.*, Influences of TSR on Gaseous Hydrocarbon Components and Carbon Isotopes: Revelations from High-Temperature and High-Pressure Simulation Experiments, (in Chinese), *Petroleun Geology & Experiment, 34* (2012), 1, pp. 66-70
[16] Amrani, A., *et al.*, The Role of Labile Sulfur Compounds in Thermochemical Sulfate Reduction, *Geochimica et Cosmochimica Acta, 72* (2008), 12, pp. 2960-2972
[17] Hao, F., *et al.*, The Fate of CO_2 Derived from Thermochemical Sulfate Reduction(TSR) and Effect of TSR on Carbonate Porosity and Permeability, Sichuan Basin, (in Chinese), *China, Earth Science Reviews, 141* (2015), 5, pp. 154-177
[18] Kelemen, S. R., *et al.*, Characterization of Solid Bitumens Originating from Thermal Chemical Alteration and Thermochemical Sulfate Reduction, *Geochimica et Cosmochimica Acta, 74* (2010), 18, pp. 5305-5332
[19] Zhao, H., *et al.*, Study of Thermochemical Sulfate Reduction of Different Organic Matter: Insight from Systematic TSR Simulation Experiments, *Marine and Petroleum Geology, 100* (2019), 2, pp. 434-446
[20] Mankiewicz, P. J., *et al.*, Gas Geochemistry of the Mobile Bay Jurassic Norphlet Formation: Thermal Controls and Implications for Reservoir Connectivity, *Am. Assoc. Pet. Geol. Bull, 93* (2009), 10, pp. 19-1346
[21] Gvirtzman, Z., *et al.*, Compound-Specific Sulfur Isotope Analysis of Thiadiamondoids of Oils from the Smackover Formation, USA, *Geochimica et Cosmochimica Acta, 167* (2015), 10, pp. 144-161
[22] Zhu, G. Y., *et al.*, Discovery of the Lower Cambrian High-Quality Source Rocks and Deep Oil and Gas Exploration Potential in the Tarim Basin, China, *Am. Assoc. Pet. Geol. Bull, 102* (2018), 10, pp. 2123-2151
[23] Li, K. K., *et al.*, Fluid Inclusion and Stable Isotopic Studies of Thermochemical Sulfate Reduction: Upper Permian and Lower Triassic Gas fields, Northeast Sichuan Basin, China, *Geochimca Cosmochimca Acta, 246* (2019), 1, pp. 86-108
[24] Jenden, P. D., *et al.*, Enrichment of Nitrogen and ^{13}C of Methane in Natural Gases from the Khuff Formation, Saudi Arabia, Caused by Thermochemical Sulfate Reduction, *Organic Geochemistry, 82* (2015), 5, pp. 54-68
[25] Wang, Y., *et al.* A Variational Formulation for Anisotropic Wave Traveling in a Porous Medium, *Fractals, 27* (2019), June, 1950047
[26] Wang, K. L., He, C. H., A Remark on Wang's Fractal Variational Principle, *Fractals, 27* (2019), 8, ID 1950134
[27] Wang, Y., Deng, Q. G., Fractal Derivative Model for Tsunami Traveling, *Fractals, 27* (2019), 2, 1950017
[28] Wang, Y., *et al.*, A Fractal Derivative Model for Snow's Thermal Insulation Property, *Thermal Science, 23* (2019), 4, pp. 2351-2354
[29] He, J. H., Fractal Calculus and Its Geometrical Explanation, *Results in Physics, 10* (2018), Sep., 272-276
[30] He, J. H., A Simple Approach to One-Dimensional Convection-Diffusion Equation and Its Fractional Modification for E Reaction Arising in Rotating Disk Electrodes, *Journal of Electroanalytical Chemistry, 854* (2019), 113565
[31] Wang, Q. L., *et al.* Fractal Calculus and Its Application to Explanation of Biomechanism of Polar Bear hairs, *Fractals, 26* (2018), 6, 1850086
[32] Wang, Q. l., *et al.* Fractal calculus and Its Application to Explanation of Biomechanism of Polar Bear Hairs (vol. 26, 1850086, 2018), *Fractals, 27* (2019), 5, ID 1992001

[33] He, J. H., Ji, F. Y., Two-Scale Mathematics and Fractional Calculus for Thermodynamics, *Thermal Science, 23* (2019), 4, pp. 2131-2133
[34] Ain, Q. T., He, J. H., On Two-Scale Dimension and Its Applications, *Thermal Science*, (2019), 3B, pp. 1707-171*223*
[35] Fan, J., *et al.*, Fractal Calculus for Analysis of Wool Fiber: Mathematical Insight of Its Biomechanism, *Journal of Engineered Fibers and Fabrics*, On-line first, https://doi.org/10.1177/1558925019872200, 2019

Paper submitted: April 24, 2019
Paper revised: September 21, 2019
Paper accepted: September 21, 2019